13.2 EVOLUTION OF ANALYSIS ERROR AND ADJOINT-BASED OPTIMAL PERTURBATION IN A QUASIGEOSTROPHIC MODEL

Hyun Mee Kim* and Michael C. Morgan
University of Wisconsin-Madison, Madison, Wisconsin

1. INTRODUCTION

Numerical weather prediction (NWP) forecast error is attributed to imperfections of the forecast model and to uncertainties in the initial conditions of the forecast model. For short term forecasts, the growth of initial condition uncertainty (so-called "intrinsic error") has been recognized as the biggest contributor to forecast error. Given a perfect model, the growth of the forecast error in a modeled flow depends on the susceptibility of perturbations in that flow to amplify.

The dynamical mechanism of the intrinsic error growth and propagation in a NWP system has been partially explained by the mechanisms of singular vector (SV) development. SVs, the fastest growing perturbations over a specified time period for a given basic state for a specific norm, are an appropriate tool to assess the susceptibility of fluid flows to rapid perturbation growth (e.g., Farrell 1989). Since the amplification of SVs are constrained by a predefined norm, different SV development mechanisms can be identified depending on which norm is chosen: the most commonly chosen norms have been streamfunction variance, potential enstrophy, and total energy. The fundamental mechanism for SV development has been studied by investigating the amplification of streamfunction variance SVs (e.g., Morgan 2001), and potential enstrophy and energy SVs (e.g., Kim and Morgan 2002) within simple Eady-type basic states. For the streamfunction variance and energy SVs, a three-stage sequence describes the SV development. The first stage of SV development is associated with superposition of the initially upshear tilted interior potential vorticity (PV) by the baroclinic shear. Subsequently the initially small boundary potential temperature (PT) anomalies are intensified by the winds attributed to the PV and finally these amplified boundary PT anomalies interact with each other to sustain the growth. For the potential enstrophy SVs, however, the mutual interaction between the boundary PT anomalies is the primary mechanism for SV evolution from the beginning and the interior PV may not play a significant role during the development.

Despite these explanations of perturbation growth, the growth and propagation mechanisms of intrinsic error are still recognized as a partially resolved problem since the above studies focus mostly on SV growth but do not investigate the evolution of the initial condition error and the possible similarity of the evolution of the initial condition error and the SV development.

In this presentation, using piecewise PV inversion and localized E-P flux diagnostics, the structure and subsequent evolution of a realization of the intrinsic error are diagnosed and compared with those of the potential enstrophy SV. In order to fully exploit the error growth and propagation in terms of its interaction with the basic state, the three-dimensional quasigeostrophic (QG) model developed at the National Center for Atmospheric Research (NCAR) (Snyder et al. 2003) is used. The adjoint model developed for this QG model (Kim 2002) is used to calculate SVs. Section 2 contains a brief description of model. The case selected and generation of the perturbations (error and SV) for the experiment are presented in section 3. The piecewise PV, localized E-P flux, and combined PV and localized E-P flux diagnostics are presented in section 4. More detailed formulations and explanations of the experimental framework and diagnostics can be found in Kim (2002). The evolution of the error and SV are presented in sections 5 and 6 respectively. Section 7 describes the role of barotropic and baroclinic processes during the evolution of the error and SV. Section 8 contains a summary and discussion.

2. MODEL

The model is a zonally periodic QG grid point channel model with rigid top and bottom surfaces on a beta plane. The model variables are PV in the interior and PT at the upper and lower boundaries. The main forcing is a relaxation to a specific zonal mean reference state which is the Hoskins - West jet (Hoskins and West 1979). There is no orography or seasonal cycle and it has fourth order horizontal diffusion by numerical smoothing and Ekman pumping at the lower boundary. Stratification is constant and the tropopause is fixed with varying temperature. The model is discretized into 5 levels in a troposphere of 9 km depth. The horizontal resolution of the domain which is 16000 km in circumference and 8000 km in width is 250 km.

3. EXPERIMENTAL STATES

3.1 *Error*

A case is selected based on its similarity to a midlatitude cyclogenesis situation from a set of states integrated forward using the nonlinear QG model. We identify this arbitrary trajectory as the *true* state of our idealized experiment. A *model* state is initially generated from the true state modified by random noise and subsequently

**Corresponding author address:* Dr. Hyun Mee Kim, University of Wisconsin-Madison, Department of Atmospheric and Oceanic Sciences, 1225 W. Dayton Street, Madison, Wisconsin, 53706; e-mail: khm@mapmaker.aos.wisc.edu

made by assimilating simulated rawinsonde observations to the previous forecast using three-dimensional variational data assimilation system. The *analysis error* is defined as the difference between the true and model states at the initial time. The *forecast error* is defined by the difference between the true and model states at subsequent times. The three-dimensional variational data assimilation scheme, simulated rawinsonde observations, and observational error characteristics are described in Morss et al. (2001).

3.2 *Singular vector*

The calculation of SVs essentially involves selecting a initial disturbance which grows most rapidly in a specified norm after some finite optimization time, $t = \tau_{opt}$. In this study, we choose the norm as the potential enstrophy since the model state vector is constructed by the PV in the interior of the model domain and the PT at the upper and lower boundaries. The potential enstrophy is defined similar to Kim and Morgan (2002). The constrained optimization problem seeks to maximize the Rayleigh quotient, λ,

$$\lambda = \frac{\mathbf{x}'(t_0)^T \mathbf{M}^T \mathbf{M} \mathbf{x}'(t_0)}{\mathbf{x}'(t_0)^T \mathbf{x}'(t_0)}, \tag{1}$$

at time $t = \tau_{opt}$ where $\mathbf{x}'(t_0)$ is the initial perturbation and $\mathbf{M}^T$ is the adjoint model of the forward tangent propagator $\mathbf{M}$. It may be shown that the maximum of this ratio is realized when $\mathbf{x}'(t_0)$ is the SV of the forward tangent propagator $\mathbf{M}$ for the potential enstrophy norm. A Lanczos type algorithm is used to solve for $\mathbf{x}'(t_0)$ in (1). Because the adjoint of the forward tangent propagator of a given nonlinear model is used to calculate the SVs, SVs are called *adjoint-based perturbation*.

4. DIAGNOSTICS

4.1 *Potential vorticity diagnosis*

A diagnosis of perturbation development and the nonlinear feedback between the perturbation and basic state in the QG model requires identifying the interactions between interior PV anomalies at a given height (or boundary PT anomalies) in the domain with the basic state at other heights. For this purpose, piecewise PV inversion is used and the PV (perturbation PV) is partitioned into three parts: lower PT (PT anomalies), interior PV (PV anomalies), and upper PT (PT anomalies). Based on this partition, we may partition the perturbation streamfunction into those parts associated with the boundary PT anomalies and those parts associated with the interior PV anomalies. The zonal (meridional) velocities attributed to the PV anomalies and boundary PT anomalies respectively may be calculated from the partitioned streamfunction.

4.2 *Localized E-P flux diagnosis*

An alternate diagnosis of the perturbation development and the interaction between the perturbation and basic state may be afforded by an E-P flux diagnosis. For application to the three-dimensional QG model, the localized E-P flux derived on the time-mean basic state is used with the Wentzel-Kramers-Brillouin-Jeffreys (WKBJ) approximation which requires that the time variations of the basic state are sufficiently slow compared with the time variations of the perturbations. The $\mathbf{E}$ vectors in Trenberth (1986) are used to diagnose the interaction between the perturbation and basic state and presented as

$$\mathbf{E} = \left[\frac{1}{2}(\overline{v'^2} - \overline{u'^2}), -\overline{u'v'}, \frac{f}{N^2}\overline{v'\theta'}\right]. \tag{2}$$

The $\mathbf{E}$ vectors indicate the relative magnitudes of the perturbation heat and momentum transports and the information concerning Rossby wave group velocity associated with these perturbations. The $\mathbf{E}$-vector divergence (convergence) denotes the extent to which the perturbation heat and momentum fluxes accelerate (decelerate) the time-mean basic flow. On the other hand, since the perturbation and the time-mean basic flow interact each other, the $\mathbf{E}$-vector divergence (convergence) may be used as a diagnostic of the basic state forcing to decrease (increase) the amplitude of perturbations.

4.3 *Combined PV and localized E-P flux diagnosis*

By combining PV inversion and the localized E-P flux diagnostics, the various error development mechanisms may be apprehended. After all the variables in (2) are partitioned into the components attributed to the interior PV and boundary PTs, the localized E-P flux can be partitioned as three interaction terms, $\mathbf{E}_{q'-q'}$, $\mathbf{E}_{q'-\theta'}$, and $\mathbf{E}_{\theta'-\theta'}$. The $\mathbf{E}_{q'-q'}$ term may be used to diagnose the interaction between the interior PVs such as baroclinic or barotropic PV superposition. The $\mathbf{E}_{q'-\theta'}$ term is associated with the interaction between the interior PV and boundary PTs such as the advection of the boundary PTs (interior PV) by winds attributed to the interior PV (boundary PTs). The $\mathbf{E}_{\theta'-\theta'}$ term can be used to diagnose the mutual interactions between the PTs on upper and lower boundaries. The E-P flux can be written as

$$\mathbf{E} = \mathbf{E}_{q'-q'} + \mathbf{E}_{q'-\theta'} + \mathbf{E}_{\theta'-\theta'}, \tag{3}$$

where

$$\begin{aligned}
\mathbf{E}_{q'-q'} &= \left[\frac{1}{2}(\overline{v_q'^2} - \overline{u_q'^2}), -\overline{u_q'v_q'}, \frac{f}{N^2}\overline{v_q'\theta_q'}\right], \\
\mathbf{E}_{q'-\theta'} &= \left[\overline{v_q'v_\theta'} - \overline{u_q'u_\theta'}, -\overline{u_q'v_\theta'} - \overline{u_\theta'v_q'}, \frac{f}{N^2}(\overline{v_q'\theta_\theta'} + \overline{v_\theta'\theta_q'})\right], \\
\mathbf{E}_{\theta'-\theta'} &= \left[\frac{1}{2}(\overline{v_\theta'^2} - \overline{u_\theta'^2}), -\overline{u_\theta'v_\theta'}, \frac{f}{N^2}\overline{v_\theta'\theta_\theta'}\right].
\end{aligned}$$

5. EVOLUTION OF THE ERROR

Given a perfect model, there are two scenarios leading to large forecast error at the verification time. Those errors which project onto the amplifying SVs of the flow grow very rapidly during the evolution. This kind of error will be referred to as a "Type A" error. The other scenario is that those initially large errors which do not project onto the amplifying SVs contribute to large forecast error by remaining large or slowly amplifying. This is a case of “Type B” error.

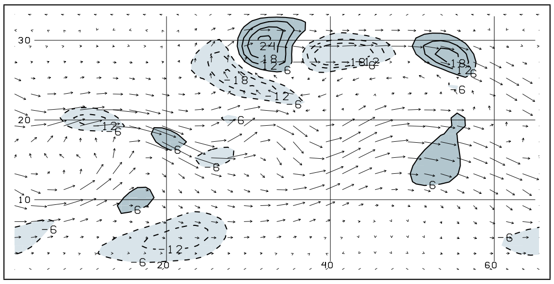

(a) 0h analysis error ($\|\mathbf{x}'\|$ = 7.35)

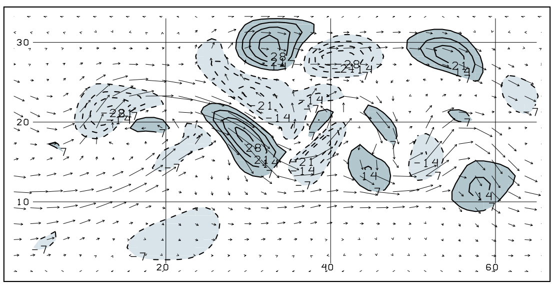

(b) 24h forecast error ($\|\mathbf{x}'\|$ = 8.91)

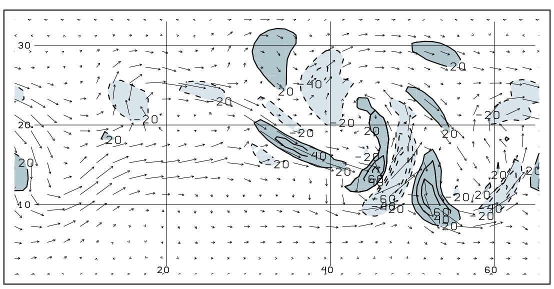

(c) 48h forecast error ($\|\mathbf{x}'\|$ = 15.05)

FIG. 1. Horizontal cross-sections of the lower boundary PT error (contours and filled), lower tropospheric wind shear (level 4 to the bottom) (arrows) at the selected times: (a) 0h, (b) 24h, and (c) 48h. The magnitudes of errors in the parentheses are obtained for the entire domain.

From now on we focus on the development of the lower boundary PT error since the results of diagnostics on the upper boundary are quite similar to those on the lower boundary. Figure 1 shows the lower boundary PT error and the lower tropospheric wind shear (level 4 to the bottom) at times t = 0h, 24h, and 48h. The error is initially characterized by structures with small amplitude in the middle of the domain and larger amplitude near the northern and southern boundaries. Shortly after the initial time, the Type A error begins to grow rapidly while showing evidence of downstream development. The growth and propagation of the Type B error are relatively small compared to the Type A error. The error amplifies by a factor of 2.05 for 48 hours for the entire domain.

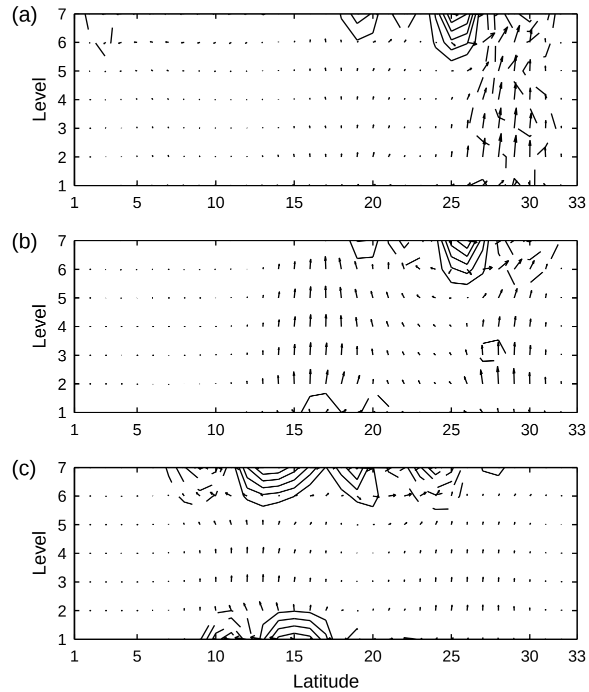

FIG. 2. Longitudinally averaged vertical cross-section of the three-dimensional $\mathbf{E}$-vector divergence (solid line), convergence (dashed line), and the meridional and vertical components of the $\mathbf{E}$ vectors (arrow) associated with the error at the selected times: (a) 0h, (b) 24h, and (c) 48h.

The WKBJ approximation may be used to diagnose the error evolution since the amplitude of the basic state varies slowly compared with the amplitude of the errors. Vertical cross-sections of the longitudinally averaged three-dimensional $\mathbf{E}$-vector divergence and the meridional and vertical components of the $\mathbf{E}$ vector at times t = 0h, 24h, and 48h are shown in Fig. 2. The meridional and vertical components of the $\mathbf{E}$ vector are directed upward over most of the domain throughout the evolution. The $\mathbf{E}$-vector convergence and concentrated upward $\mathbf{E}$ vectors near the northern boundary at t = 0h indicate the large Type B error (Fig. 2a). As seen in Fig. 2b, the $\mathbf{E}$ vectors begin to appear in the middle of the domain at t = 24h (Fig. 2b). Contrary to the $\mathbf{E}$-vector convergence (Type B error growth) initially indicated near the northern boundary, the $\mathbf{E}$-vector divergence is found at the top and bottom in the middle of the domain at t = 48h, which implies that the basic states' modulation by perturbations might be the main mechanism of the Type A error growth (Fig. 2c). The basic states' modulation by perturbations is associated with either phase (e.g., Snyder 1999) or amplitude errors of the basic state. The orientation and magnitude of $\mathbf{E}_{\theta'-\theta'}$ vectors and the pattern of divergence are very similar to those of the total $\mathbf{E}$ flux implying that most of the total $\mathbf{E}$ flux may be explained by the mutual interactions between upper and lower boundaries (not shown). The magnitudes of $\mathbf{E}_{q'-q'}-$vector and $\mathbf{E}_{q'-\theta'}-$vector are $1 \sim 2$ orders less than that of the $\mathbf{E}_{\theta'-\theta'}$ vector.

In summary, the $\theta' - \theta'$ component of $\mathbf{E}$ flux explains most of the total $\mathbf{E}$ flux implying that the mutual interaction between the PTs on upper and lower boundaries is the primary mechanism of the error growth and propagation. At the early stage of the development, however, the barotropic processes are suspected even though the $\mathbf{E}$ vectors are mainly vertical.

6. EVOLUTION OF THE SINGULAR VECTOR

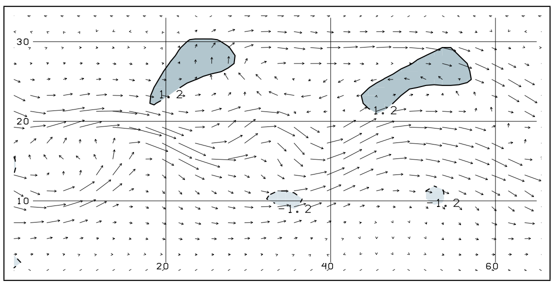

(a) 0h SV ($\|\mathbf{x}'\|$ = 1.00)

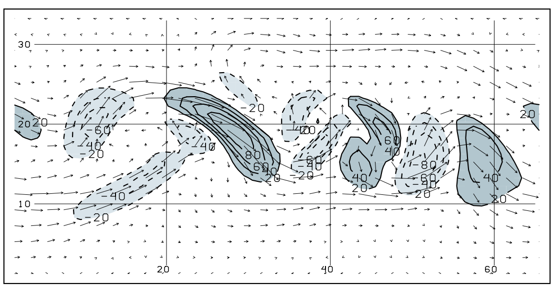

(b) 24h evolved SV ($\|\mathbf{x}'\|$ = 29.36)

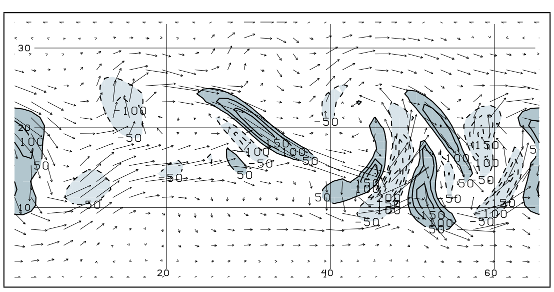

(c) 48h evolved SV ($\|\mathbf{x}'\|$ = 70.27)

FIG. 3. Horizontal cross-sections of the lower boundary SV PT (contours and filled), lower tropospheric wind shear (level 4 to the bottom) (arrows) at the selected times (a) 0h, (b) 24h, and (c) 48h. The magnitudes of the SV in the parentheses are obtained for the entire domain.

Figure 3 shows the lower boundary SV PT and the lower tropospheric wind shear (level 4 to the bottom) at the indicated times. The SV PV is initially characterized by structures with small amplitude in the middle of the domain and larger amplitude near the northern boundary partially identifying the Type B error (Fig. 3a). Shortly after the initial time, the SV begins to grow rapidly near the jet (Fig. 3b). The Type B error near the northern boundary is not identified by the SV after t = 24h. The SV amplifies by a factor of 70.27 for 48 hours for the entire domain.

The presence of barotropic processes are confirmed by the orientation of the $\mathbf{E}$ vectors from the northern and southern boundaries into the middle of the domain at t = 0h (Fig. 4a). After t = 24h, the $\mathbf{E}$ vectors are directed from the lower boundary to the upper boundary in the middle of the domain (Figs. 4b and c). The orientation and magnitude of $\mathbf{E}_{\theta'-\theta'}$ vectors and the pattern of divergence are very similar to those of the total $\mathbf{E}$ fluxes implying that most of the total $\mathbf{E}$ fluxes may be explained by the barotropic processes and following baroclinic processes between the PTs on upper and lower boundaries (not shown).

In summary, the $\theta' - \theta'$ component of $\mathbf{E}$ flux explains most of the total $\mathbf{E}$ flux implying that the mutual interactions between the PTs on the upper and lower boundaries are the primary mechanism of the SV growth and propagation. Different from the $\mathbf{E}$ flux of the error, the strong barotropic processes are clearly observed by the orientation of the $\mathbf{E}$ vectors at the initial stage of the evolution.

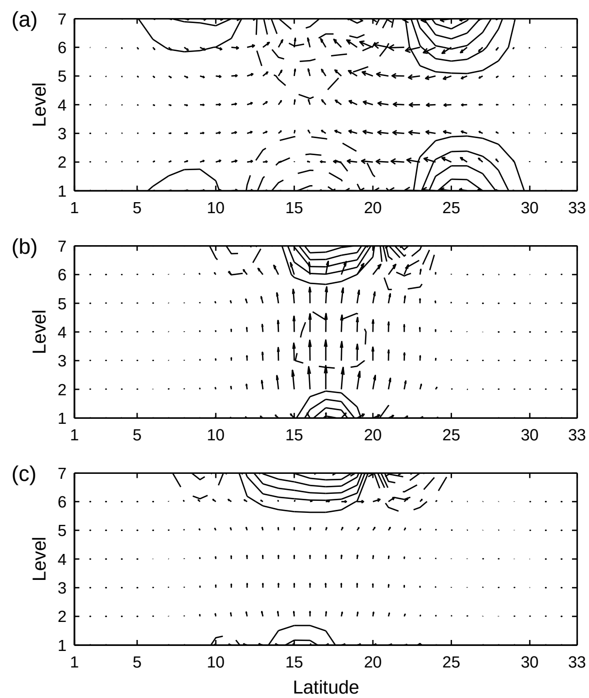

FIG. 4. Longitudinally averaged vertical cross-section of the three-dimensional $\mathbf{E}$-vector divergence (solid line), convergence (dashed line), and the meridional and vertical components of the $\mathbf{E}$ vectors (arrow) associated with the SV at he selected times: (a) 0h, (b) 24h, and (c) 48h.

7. BAROTROPIC AND BAROCLINIC PROCESSES

From the localized E-P flux diagnostics, the $\theta' - \theta'$ component of $\mathbf{E}$ flux explains most of the total $\mathbf{E}$ flux for the error and SV during the evolution, which implies that a baroclinic process (i.e., the interaction between the upper and lower boundaries) is an important mechanism of the perturbation growth and propagation for this case. The effect of barotropic processes, however, are suggested in the early stage of the perturbation evolution. For the error, barotropic processes are suspected for the first 24 hours of the evolution but not clearly indicated by the orientation of the $\mathbf{E}$ vectors (Figs. 2a and b). The barotropic processes are clearly indicated by $\mathbf{E}$ vectors of the SV at t = 0h (Fig. 4a).

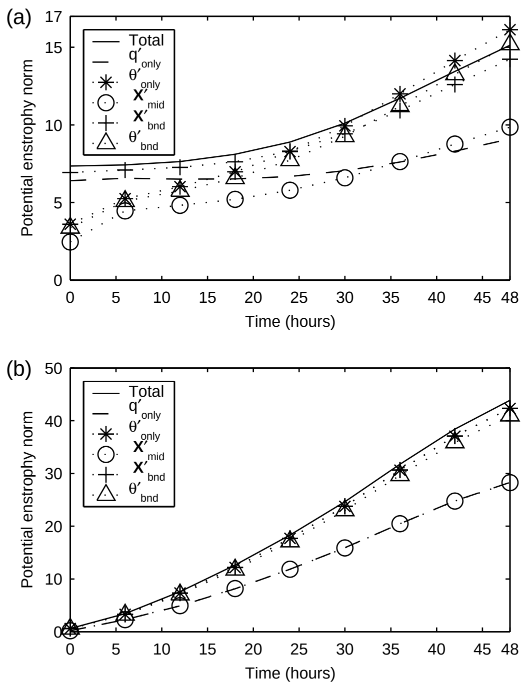

FIG. 5. (a) Time evolution of Total error, q'_{only} error, θ'_{only} error, $\mathbf{x}'_{mid}$ error from the grid point 16 to 22 meridionally, $\mathbf{x}'_{bnd}$ error from the grid point 0 to 15 and 23 to 33 meridionally, and θ'_{bnd} error from grid point 0 to 15 and 23 to 33 meridionally. (b) Time evolution of the Total SV, q'_{only} SV, θ'_{only} SV, $\mathbf{x}'_{mid}$ SV from the grid point 13 to 19 meridionally, $\mathbf{x}'_{bnd}$ SV from the grid point 0 to 12 and 20 to 33 meridionally, and θ'_{bnd} SV from grid point 0 to 12 and 20 to 33 meridionally.

The relative importance of the barotropic or baroclinic processes during the perturbation evolution can be demonstrated by eliminating particular parts of the PV in the initial perturbation structure, and allowing the modified structure to develop. Six initial configurations of PV perturbations are chosen: the perturbation state vector (Total), a perturbation with only initial interior PV (q'_{only}) of the total state vector, a perturbation with only initial boundary PT (θ'_{only}) of the total state vector, a perturbation with only initial state vector in the middle of the domain ($\mathbf{x}'_{mid}$) of the total state vector, a perturbation with only initial state vector near the northern and southern boundaries ($\mathbf{x}'_{bnd}$) of the total state vector, and a perturbation with only initial boundary PT near the northern and southern boundaries (θ'_{bnd}) of the total state vector.

The evolutions of the six initial perturbations in L_2 norm which is potential enstrophy norm in this case are shown in Fig. 5. For the error, the initially small θ'_{only} becomes larger than the q'_{only} after t = 15h implying that the mutual interactions of both upper and lower boundaries are an important mechanism of the error growth for relatively later stage of the evolution (Fig. 5a). While the $\mathbf{x}'_{mid}$ shows small amplitude during the evolution, the $\mathbf{x}'_{bnd}$ grows very close to the total perturbation during the evolution implying that the initial errors near the meridional boundaries are more important for the final time error than those errors initially located in the middle of the domain. Initially large q'_{only} and $\mathbf{x}'_{bnd}$ indicate the large Type B error near the northern and southern boundaries. Even though θ'_{bnd} is initially much less than $\mathbf{x}'_{bnd}$, θ'_{bnd} is comparable to θ'_{only} during the evolution implying that the upper and lower boundaries near meridional boundaries are important for the Type A error growth.

For the SV, both barotropic and baroclinic processes are important for the perturbation growth from the beginning (Fig. 5b). While the magnitude of θ'_{only} is the closest to that of the total perturbation, the magnitude of θ'_{bnd} is slightly less than that of θ'_{only} implying that the most of the growth can be explained by the barotropic processes occurring at the upper and lower boundaries from the northern and southern boundaries into the middle of the domain and following baroclinic processes between the upper and lower boundaries in the middle of the domain.

8. SUMMARY AND DISCUSSION

In this presentation, the initial structures and subsequent evolution of the error and SV within a QG model have been diagnosed. Based on the results of a piecewise PV inversion and a partitioning of the localized E-P fluxes associated with each perturbation, it has been demonstrated that the mechanisms for error growth and propagation depend upon projection of error onto the rapidly growing structure (i.e., SV) of the flow. Barotropic processes as well as the baroclinic processes are observed depending on the projection of individual perturbations onto SV during the evolution. Below we briefly summarize and interpret the results separately for each of the perturbations studied.

The Type A error, which is a rapidly growing perturbation, grows by a two stage process. At the early stage of the evolution, the development is characterized by the barotropic processes from the meridional boundaries into the middle of the domain. Following the barotropic growth processes, baroclinic processes, associated with interactions between thermal anomalies along the upper and lower boundaries in the middle of the domain, explain most of the error growth at the later stage of the evolution. The Type B error, which is initially large and does not project onto SV, does not grow and propagate compared to the Type A error and explains most of the error at the early stage of the evolution.

For the SV, the interior PV plays a relatively small role in the perturbation amplification. The strong barotropic processes which are observed at the early stage of the evolution are mostly caused by the perturbations at the upper and lower boundaries near the northern and southern boundaries not in the interior. Following the barotropic processes at the very initial stage, the baroclinic processes between the upper and lower boundaries are the primary mechanism of the SV growth. The transition between the barotropic and baroclinic processes of SV occurs in a very short period compared to that of the error, which is expected from the rapid concentration of SV $\mathbf{E}$-vector divergence in the middle of the domain after the initial time. The SV represents the rapidly growing error very well during the evolution and may be used as a surrogate of that rapidly growing part of the error for adaptive observation or data assimilation purposes.

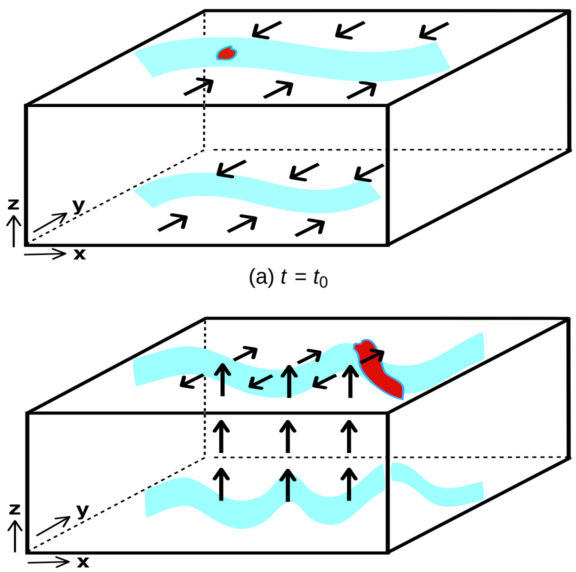

(b) $t > t_0$

FIG. 6. Schematic diagram of the error growth and propagation mechanisms: (a) barotropic processes at the initial time and (b) baroclinic processes followed by slight barotropic processes at the final time. Arrows indicate the $\mathbf{E}$ vectors and shadings represent the regions of large PV gradient. The initially small error (indicated by the small structure in (a)) near the baroclinically unstable region grows rapidly and becomes large error (indicated by large structure in (b)) at the final time.

The current study demonstrates that the barotropic transport of wave activity from regions of small PV gradient (i.e., near the northern and southern boundaries remote from the jet in this study) to regions of large PV gradient (i.e., near the jet in the middle of the domain) along the upper and lower boundaries are important for the growth and propagation of the error and SV at the early stage of the evolution. The baroclinic transport of wave activity from the lower boundary to the upper boundary becomes important at the later stage of the development. The initial barotropic processes are concentrated along the upper and lower boundaries since the meridional PV gradient is weak in the interior of the domain. The schematic diagram of the error growth and propagation mechanisms is shown in Fig. 6. Because of the barotropic error growth and propagation mechanism along the upper and lower boundaries at the early stage of the evolution, the adaptive observations concentrated in the sensitive regions remote from the baroclinically unstable region of the flow would be effective in reducing a subsequent forecast error as long as those sensitive regions are indicated by the SV.

Acknowledgments

The authors wish to thank Dr. Matthew Hitchman for insightful discussions regarding the E-P flux diagnostics. The authors thank Linda Keller for helpful comments on an earlier version of this manuscript. This work was supported by the National Science Foundation grants ATM-9810916 and ATM-0121186.

REFERENCES

Farrell, B., 1989: Optimal excitation of baroclinic waves. *J. Atmos. Sci.*, **46**, 1193–1206.

Hoskins, B. J. and N. V. West, 1979: Baroclinic waves and frontogenesis. Part II: Uniform potential vorticity jet flows - cold and warm fronts. *J. Atmos. Sci.*, **36**, 1663–1680.

Kim, H. M., 2002: *Diagnosis of error growth and propagation: Implications for adaptive observations.*, PhD thesis, University of Wisconsin-Madison, 197 pp. [Available online at *http://aurora.aos.wisc.edu/∼khm /manuscripts/thesis.pdf*.].

Kim, H. M. and M. Morgan, 2002: Dependence of singular vector structure and evolution on the choice of norm. *J. Atmos. Sci.*, **59**, 3099–3116.

Morgan, M., 2001: A potential vorticity and wave activity diagnosis of optimal perturbation evolution. *J. Atmos. Sci.*, **58**, 2518–2544.

Morss, R. E., K. A. Emanuel, and C. Snyder, 2001: Idealized adaptive observation strategies for improving numerical weather prediction. *J. Atmos. Sci.*, **58**, 210–232.

Snyder, C., 1999: Error growth in flows with finite-amplitude waves or coherent structures. *J. Atmos. Sci.*, **56**, 500–506.

Snyder, C., T. M. Hamill, and S. B. Trier, 2003: Linear evolution of error covariances in a quasigeostrophic model. *Mon. Wea. Rev.*, **131**, 189–205.

Trenberth, K. E., 1986: An assessment of the impact of transient eddies on the zonal flow during a blocking episode using localized Eliassen-Palm flux diagnostics. *J. Atmos. Sci.*, **43**, 2070–2087.